Journal of ELECTRICAL ENGINEERING, VOL 70 (2019), NO-7S, 89–94

sciendo

PAPERS

Superconducting properties of very high quality NbN thin films grown by pulsed laser deposition

Serhii Volkov, Maros Gregor, Tomas Roch, Leonid Satrapinskyy, Branislav Grančič, Tomas Fiantok, Andrej Plecenik*

In this work, we study the effect of the various substrates on the growth and superconducting properties of NbN thin films grown by using pulsed laser ablation in a $N_2 + 1\%H_2$ atmosphere on MgO, Al_2O_3 and Si substrates. Structural and superconducting analyses of the films demonstrate that using MgO and Al_2O_3 substrates can significantly improve the film properties compared to Si substrate. The X-ray diffraction data indicate that MgO and Al_2O_3 substrates produce highly oriented superconducting NbN films with large coherent domain size in the out-of plane direction on the order of layer thickness and with a superconducting transition temperature of 13.1 K and 15.2 K, respectively. On the other hand, the NbN film grown on the Si substrate exhibits random polycrystalline orientation. Together with the smallest coherent domain size it leads to the lower critical temperature of 8.3 K. Finally, by using a passivation surface layer we are able to improve superconducting properties of NbN thin film and we observe superconducting transition temperature 16.6 K, the one of the highest value reported so far for 50 nm thick NbN film on sapphire.

K e y w o r d s: high-quality NbN films, deposition of niobium nitride, pulsed laser deposition of NbN films

1 Introduction

Despite of great efforts at investigation of high-temperature superconductors, the classical superconductors, such as niobium nitride (NbN), are still attractive in many applications. NbN is widely used in superconducting electronics circuits, quantum computing and high-frequency devices [1] (such as high-sensitive single-photon detectors and SQUID systems) due to relatively high superconducting critical temperature (T_c) near 16 K, energy gap $\Delta \approx 2.46$ meV in the fcc phase [2] and high upper critical magnetic field $B_{c2} \sim 40$ T.

NbN can be formed in hexagonal, tetragonal, or cubic crystal structures [3]. Due to this polymorphism and a high affinity to oxygen, the NbN is very sensitive to the deposition conditions and to achieve very good superconducting properties of thin films (below 50 nm) with the high T_c is still a great challenge.

NbN thin films are generally fabricated by reactive magnetron sputtering [4], high-temperature chemical vapor deposition technique (HTCVD) [5] or atomic layer deposition (ALD) [6]. Olaya et. al. [4] deposited NbN films using the reactive magnetron sputtering at the substrate temperature up to 650 °C and they showed that by increasing of the grain size from 15 to 35 nm, the critical temperature increase from 12.6 to 16 K for relatively thick 1.8 μm NbN sample. Hazra et. al. [5] fabricated 40 nm thin NbN film with $T_c = 16.8$ K at sapphire by using of high-temperature chemical vapor deposition technique with the high substrate temperature (T_s) of 1300 °C, which makes this technology unusable for the preparation of heterostructures. On the other hand, Linzen [6] reported the fabrication of high quality 40 nm thick NbN film deposited by plasma-assisted ALD with relatively lower substrate temperature of $T_s = 350$ °C on sapphire, but with lower T_c of 13.8 K.

Recently, a lot of investigations have been carried out to fabricate thin NbN films by using pulsed laser deposition (PLD) mostly on the MgO substrate with relatively high T_s and a middle laser fluency about 6 J cm^{-2} [7-9]. In this case, for 40 – 50 nm thick film, the critical temperature T_c about 16.1 K has been achieved. [7, 8]. On the other hand, Kaul et. al. [9] deposited 40 nm thick NbN film on MgO and Si substrates with $T_c = 16.2$ K and $T_c = 12$ K at the room temperature but with the high laser fluency of 20 J cm^{-2}.

In this work, we compare the structure and superconducting properties of 50 nm thick NbN films grown on various substrates by PLD at the low laser fluency mode (smaller than 5 J cm^{-2}) and with the substrate temperature up to 600 °C. Using of the low laser fluency and relatively low substrate temperature allows us to prepare high quality smooth films in multilayer deposition in-situ (heterostructures), without an interdifusion between layers, which can be very useful for cryoelectronic applications.

*Department of Experimental Physics, Faculty of Mathematics, Physics and Informatics, Comenius University in Bratislava, Mlynska dolina F2, 842 48, Bratislava, Slovakia, serhii.volkov@fmph.uniba.sk

DOI: 10.2478/jee-2019–0047, Print (till 2015) ISSN 1335-3632, On-line ISSN 1339-309X

2 Experimental methods

The pulsed laser deposition of NbN films were performed in an ultra-high vacuum chamber equipped with a load-lock vacuum chamber for loading and preliminary heating of samples. A pumping system consisting of turbomolecular and scroll pumps provides the background pressure of about 8×10^{-7} Pa. The deposition was carried out using an excimer KrF laser with the wavelength of 248 nm in pulse regime, pulse duration of 35 ns, and laser fluency of 4.94 $\mathrm{J\,cm^{-2}}$. All NbN thin films were subsequently deposited from 2 inch Nb target (99.9%) in the $N_2 + 1\%H_2$ reactive atmosphere with the pressure of 9.3 Pa at gas flow of 80 sccm on heated MgO (001), Al_2O_3 (0001) and Si (001) substrates. Substrates were ultrasonically cleaned in acetone, isopropanol and deionized water. The substrate preparation process also includes short pre-annealing in the load-lock vacuum chamber and subsequently annealing in the deposition chamber up to 600 °C. Before NbN deposition, the Nb target surface was cleaned of oxygen by using 2000 extra laser pulses. During NbN deposition the substrates temperature was kept constant at 600 °C.

The NbN film deposited on the Al_2O_3 substrate was in situ covered by 50 nm NiCu layer for protection against oxidation. PLD growth of NiCu layer was performed in the pure Ar atmosphere at the pressure of 5 Pa. The substrate temperature was kept constant at 200 °C and the laser fluency was 6.42 $\mathrm{J\,cm^{-2}}$.

After deposition, NbN thin films were characterized by several analytical techniques to determine their crystal structure, chemical composition, morphology and electrical properties. Chemical composition of deposited samples was determined by energy dispersive spectroscopy system (EDS, Bruker, resolution 129 eV) at a scanning electron microscope (Tescan, Lyra) operated at energy 10 keV. The crystal structure measurement was performed by using of PANalytical X'Pert PRO MRD X-ray diffractometer with Cu Kα radiation operated at 45 kV and 40 mA applying setups for symmetric $\omega/2\theta$-scans, rocking curves (ω-scans) and grazing incidence 2θ scanning. The biaxial texture relationships between crystal lattice of deposited films and monocrystalline substrates were determined using azimuthal scans of tilted samples. Thickness of thin films was determined by X-ray reflectivity using the same diffractometer with narrow parallel beam setup. The surface morphology was analyzed by atomic force microscope (AFM, Solver 47, NT-MDT) operated in semicontact mode, with a tip curvature radius of 10 nm. Afterwards, 5 μm wide microbridges were formed from the prepared thin films using a combination of optical lithography and Ar ion beam etching. On these bridges, resistivity vs. temperature ($\rho(T)$) characteristics were then measured using standard DC four-probe measurements in a transport LHe Dewar container by utilizing Keithley 202 current source and Keithley 2000 multimeter.

3 Results and discussions

We performed XRD analysis of NbN films prepared on c-cut MgO (001), Al_2O_3 (0001) and on Si (001). Samples show fcc δ-NbN cubic structure (#01-071-0162; ICDD 1010, nominal lattice parameter $a_0 = 0.4394$ nm). Thickness values of 50 nm for the NbN layer and 50 nm for NiCu passivation layer were determined by X-ray reflectivity.

XRD $\theta/2\theta$ pattern from sample A (NbN on MgO, Fig. 1(a)) shows only very narrow and relatively strong NbN 002 and its higher order NbN 004 diffractions, which implies very high (001) preferential orientation of NbN on MgO. Diffractions NbN 111 and NbN 222 for sample B (NbN on Al_2O_3, Fig. 1(b)) have an order of magnitude higher intensity than 002 and 004 peaks for sample A, which means very strong (111) preferential orientation of NbN on Al_2O_3. Rocking curve peaks (not shown in this paper) measured around NbN reflections for sample A were order of magnitude broader (FWHM $\sim 0.9\,^\circ$, NbN 002 and 004) than for sample B (FWHM $< 0.1\,^\circ$, NbN 111 and 222). After subtracting instrumental broadening from the peak widths in rocking ω-scans and by converting into reciprocal space units ΔQ_x we were able to estimate lateral correlation length of mosaic domains. Lateral correlation length, meaning the dimension of the coherent mosaic domains in plane parallel to sample surface, is on the order of 30 nm for film A and more than 200 nm for sample B respectively. The NbN films A and B show only single fcc δ-NbN oriented phase and did not contain any detectable polycrystalline random fraction as checked by grazing incidence X-ray diffraction flat patterns without polycrystalline peaks. This also invoked strong expectation of the biaxial texture (epitaxial mosaic blocks).

Instead of full texture pole figures the inset of Fig. 1(a) shows azimuthal ϕ-scan at the diffraction position of NbN (on MgO) 111 with sample normal tilted at $\psi = 54.6\,^\circ$ with respect to scattering plane. The epitaxial orientation relationships are as follows: NbN(001) $\parallel$ MgO(001) , NbN[100] $\parallel$ MgO[100]. Inset of Fig. 1(b) shows azimuthal scan through the NbN 111 diffraction of sample B tilted $70.5\,^\circ$ from surface normal. Six peaks and position of sapphire reflections (not shown) suggest orientation relationships: NbN(111) $\parallel$ Al_2O_3(0001), NbN[1-10] $\parallel$ Al_2O_3[1-100] as sketched in Fig. 1(d). Hexagonal symmetry of Al_2O_3 surface leads to two possible variants of in-plane NbN orientations, which generate six observable peaks in the azimuthal scan. Average azimuthal peak width for sample B (1.97°) is twice as larger than for sample A (0.97°) which can origin from larger in-plane lattice mismatch between NbN(111) and Al_2O_3(0001) or X-ray beam defocusing effect due to larger tilt of sample B.

Grazing incidence XRD measurement of sample C (NbN on Si, Fig. 1(c)) shows random fcc δ-NbN crystallites orientation. Additional peaks observed at $2\theta = 62.5\,^\circ$ and $82.4\,^\circ$ are most likely related to the minor hexagonal Nb_3N_4 phase. Using Williamson-Hall analysis of the peak widths related to fcc-NbN we have estimated coherent domain size of 20 nm and microstrain of

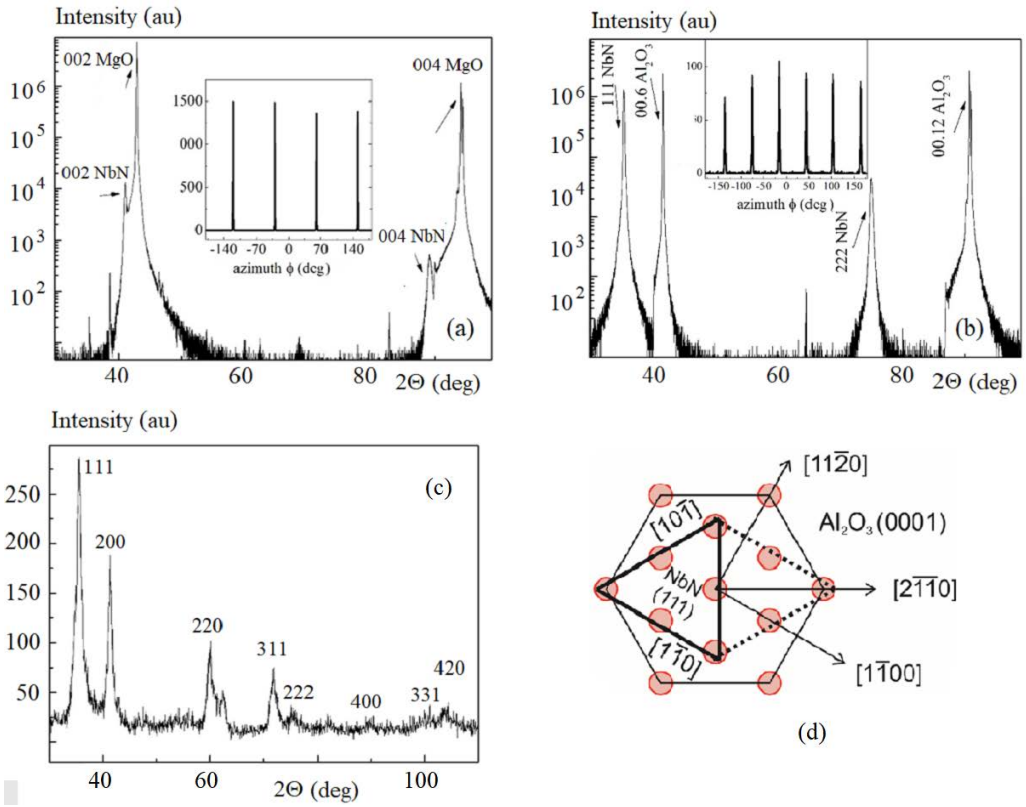

Fig. 1. XRD patterns for samples A, B and C respectively (a), (b) and (c)). Insets in the panels: (a) and (b) – the azimuthal scans at NbN 111 diffraction, (d) – lattice relation between (0001) Al_2O_3 and (111) NbN planes with two variants (dotted lines), red circles represent surface oxygen sites.

Table 1. Analyzed parameters of NbN crystal structure

Sample	Layers configuration	a_0-NbN (nm)	Average crystallite lateral size (nm)	Substrate-lattice mismatch (%)
A	MgO/NbN	0.4394	30	4.27
B	Al_2O_3/NbN	0.4379	∼200	13.1
C	Si/NbN	0.4396	20	−19.1
D	Al_2O_3/NbN/NiCu	0.4383	∼170	13.1

0.8%. Estimating from the width of NbN peaks in $\theta/2\theta$ scans the coherent domain size in the direction normal to the film surface is on the order of the film thickness. A lot more detailed results of structural analysis will be presented in our coming next paper.

Interestingly, lateral correlation length of sample B is much larger than for sample A in spite of three times larger mismatch of NbN on Al_2O_3 (Tab. 1). Lattice mismatch $m = (d_f - d_{sub})/d_{sub}$ for NbN grown on Al_2O_3 uses d-spacings of the corresponding planes $d_{NbN} = \sqrt{2}\, a_{NbN}$ and $d_{Al2O3} = 2/\sqrt{3}\, a_{Al2O3}$. As already observed for AlN [10] and NbN [11], domain matching epitaxy [12] with periodic array of misfit dislocations would allow partial relaxation. In this situation every 8 NbN atomic planes are matching 9 atomic planes of the Al_2O_3 with lattice mismatch $m = (8 \times d_{NbN} - 9 \times d_{Al2O3})/(9 \times d_{Al2O3}) = 0.5\%$.

Resistivity *vs* temperature dependencies of the NbN microbridges are presented in Fig. 2. and Tab. 2. The superconducting transition temperature (T_{con}), the zero resistivity transition temperature (T_{c0}) and the transition width ($\Delta T = T_{con} - T_{c0}$) of our NbN thin films depend on the used substrate. It can been seen, the film deposited on the sapphire substrate exhibits the highest critical temperature ($T_{con} = 15.5$ K) with a zero resistivity transition temperature of $T_{c0} = 15.2$ K followed by the film deposited on MgO ($T_{con} = 13.7$ K, $T_{c0} = 13.1$ K). On the other hand, the $\rho(T)$ measurement of sample deposited on Si shows the worst superconducting properties with $T_{con} = 10.8$ K, $T_{c0} = 8.3$ K, and with the broadest transition width of $\Delta T = 2.5$ K.

The resistivity at 20 K (ρ_{20}) of our epitaxial NbN films was in the range from 100 to 150 $\mu\Omega$cm (see Tab. 2), which is higher than values (10 – 50 $\mu\Omega$cm) reported for single-crystal NbN film [13]. Furthermore, our NbN single films showed different type of $\rho(T)$ characteristics (Fig. 2) with residual resistivity ratio RRR = ρ_{300}/ρ_{20} varying in the range from 0.82 to 1.04. As naturally expected, the residual resistivity ρ_{20} can be linked to intragrain

Table 2. The electrical parameters of investigated NbN films

Sample	Layer configuration	ρ_{300}/ρ_{20} (–)	Resistivity at 20 K, ρ_{20} ($\mu\Omega$cm)	Resistivity at 300K, ρ_{300} ($\mu\Omega$cm)	T_{con} (K)	T_{c0} (K)	ΔT_{c} (K)
A	MgO/NbN	0.8494	148	126	13.7	13.1	0.6
B	Al_2O_3 /NbN	1.042	99.6	104	15.5	15.2	0.3
C	Si/NbN	0.8242	196	162	10.8	8.3	2.5
D	Al_2O_3 /NbN/NiCu	1.071	53.8	57.6	16.6	16.4	0.2

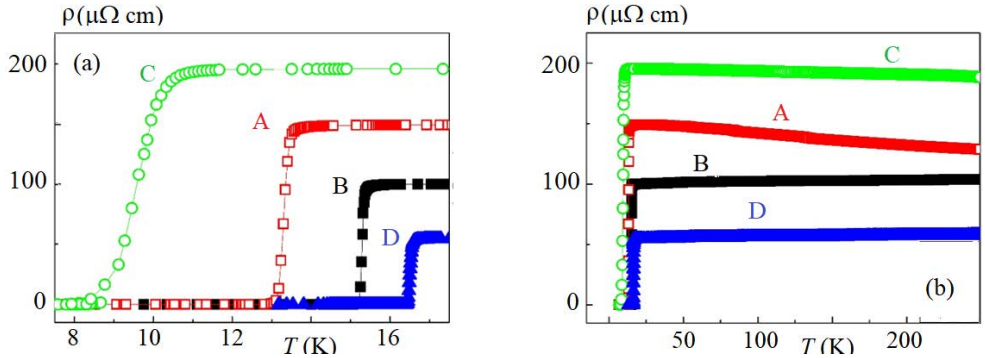

Fig. 2. $\rho(T)$ characteristics of samples: (a) – A, B, C, D viewed at low temperature range, and (b) – in wide temperature range

scattering and residual resistivity ratio reflects intergrain connectivity imperfections due to porosity and/or impurities between the grains [14]. It has been shown, that with the decrease of residual resistivity of sample, the transition temperature T_{c} increases [13].

As is seen in Fig. 2, only the sample B with the highest T_{c} shows fully metallic $\rho(T)$ characteristics with the lowest $\rho_{20} = 99.6\ \mu\Omega$cm and with RRR > 1. On the other hand, samples with the lower T_{c} (A and C) show semiconductor behavior of $\rho(T)$ characteristics with higher residual resistivity, which indicates higher concentration of scattering centers inside the grains and the RRR < 1 which implies some impurities between grains.

Even if all the samples (A, B, C) were deposited together at the same time only the sample B showed the fully metallic behavior. EDS analysis demonstrates almost the same chemical composition for all samples with Nb/N ratio to be 1.04, without any chemical contamination during the deposition.

These superconducting transport properties directly correlate with the crystal structure quality of NbN. The sample B with the best T_{c} exhibits relatively high crystallite lateral size. Although this sample has the higher lattice mismatch of 13.1% than sample A (4.27%), the domain matching effect decreases the effective lattice mismatch to only 0.5%. The sample C with the worst T_{c} has the smallest crystallite lateral size with the highest lattice – substrate mismatch of -19.1%. The T_{c} value is related not only to lattice parameter, but also to microstructure and texture of films. For instance, the best T_{c} of NbN film prepared by magnetron sputtering was observed for $a = 0.4388$ nm with Nb/N ratio near 1.09 [3]. On the other hand, the best T_{c} obtained by PLD technology on MgO was achieved for $a = 0.4428$ nm which is by 0.8% higher than reference value. In addition, different T_{c}'s were also reported for samples with almost the same stoichiometric composition [15, 16].

This effect was theoretically explained using model of the granulated superconductor as a sequence of Josephson junctions [17]. It was found, that the presence and evolution of superconductivity mainly depends on the resistivity across the grain boundaries (intergrain resistivity). As a result, we can assume that strongly-oriented thin films with the higher crystalline lateral size should have a higher T_{c} with fully metallic $\rho(T)$ characteristics due to lower number of grain boundaries and the stronger bonds at the low angle grain boundaries in comparison with randomly oriented films, which usually exhibit the semiconducting $\rho(T)$ behaviour. This has been corroborated by a number of works (see *eg* [4] and [18]) where high T_{c}'s were observed for highly-oriented samples with different grown directions [111] or [200].

The second important contribution to the T_{c} value is the coherent domain size (CDS). When the CDS is lowered to the superconducting coherence length (nanocrystaline films), it leads to suppressing of superconductivity. The T_{c} in these films can be dramatically reduced in the presence of just small concentration of inhomogeneitys and impurities. Thus, larger grain size means higher probability to obtain high T_{c} within the grains.

Another possible determinant of the superconducting transport properties of NbN thin film is a degradation. Degradation is mainly manifested as an oxidation progressing from the top of superconductive films starting

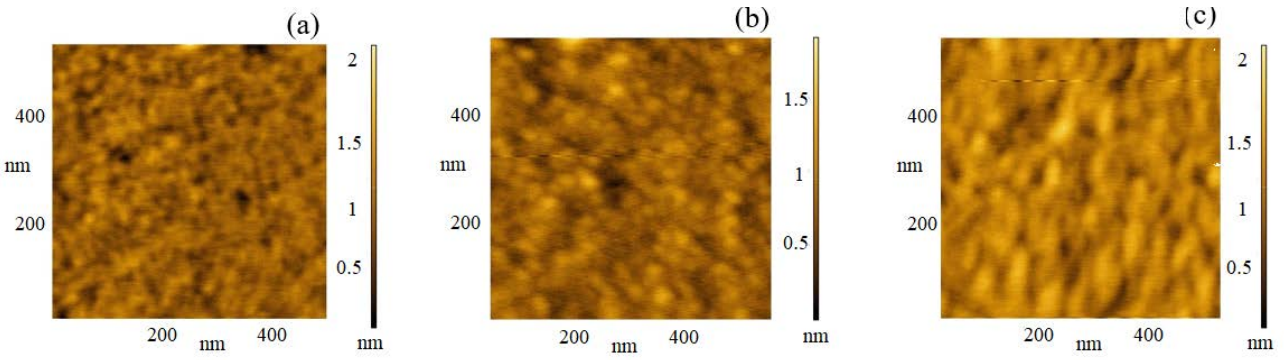

Fig. 3. Morphology of samples A, B and C ((a), (b) and (c), respectively

at the grain boundaries. It plays an extremely important role especially in the case of very thin superconductor layer because of its relatively small bulk/surface ratio. Shino et. al. obtained the increasing of T_c from 7.3 to 10.5 K for ultra-thin NbN films by using of AlN passivation layer [19]. In our case, we obtained the increasing of T_{con} for NbN films up to 16.6 K by using of NiCu passivation layer deposited in situ on NbN film (Fig. 2). Despite the fact that NiCu film was fabricated at $T_s = 200\,^\circ$C, no interdiffusion between layers was observed. It can be proved by very narrow and uniform superconductive temperature transition with the width of 0.2 K, and it does not show any additional superconductive phases (Tab. 2, Fig. 2). We performed an additional investigation of crystal structure of NbN covered by NiCu layer in order to testify that there is essentially no change of NbN crystal structure during NiCu passivation layer deposition. There was only slight increase of lattice parameter and decrease of CDS (Tab. 1). Therefore, we can conclude that the covering of NbN film by NiCu passivation layer does not lead to the structural transformation processes, which can affect the superconducting properties of individual NbN layer. We believe that increasing of T_{c0} is caused only by the protection of NbN against oxidation process.

Eventually, the atomic force microscope has been used for surface morphology analysis of deposited films (Fig. 3, Tab. 3). AFM scans on 500×500 nm area show a root-mean-square (RMS) roughness varying from 0.17 to 0.22 nm and peak to peak values from 1.90 to 2.15 nm. All samples demonstrated very small roughness with high homogeneity which permits their usage in heterostructures for various cryogenic applications.

Table 3. Morphology of 50 nm NbN films

Sample	Roughness RMS (nm)	Peak-to-Peak value (nm)
A	0.17	1.90
B	0.18	2.12
C	0.22	2.15

4 Conclusions

We have shown that superconducting properties of NbN thin films prepared by PLD technique significantly depend on the used substrates. The better structural properties with the epitaxial mosaic blocks have been grown on the c-cut Al_2O_3 and MgO substrates compared to Si substrate with random grains orientation. Although MgO has the smallest lattice mismatch with the cube-on-cube growth trend, the larger grain size has been observed on Al_2O_3 substrate. According to the literature, the hexagonal Al_2O_3 surface may allow domain matching epitaxy with the smallest lattice mismatch of 0.5% due to partial relaxation with periodic array of misfit dislocations.

The structural considerations are directly reflected in superconducting properties. The film grown on sapphire exhibits the largest grain size with the smallest residual resistivity at 20 K and fully metallic $\rho(T)$ behavior which represent tight packing of grains and good contact between them. This film has the best T_c value of 15.2 K compared to films deposited on MgO and Si with the smaller grain size, the higher residual resistivity and semiconductor $\rho(T)$ behaviour, where superconducting transition temperatures of $T_{c0} = 13.1$ K and $T_{c0} = 8.3$ K, has been measured, respectively. It is in the qualitative agreement with previous theoretical works, which estimated the influence of the grain size and resistivity inside and between grains on superconducting properties.

Due to rapid degradation of NbN thin film, 50 nm thick NiCu passivation layer has been used, by which we were able to sufficiently improve the T_c of NbN films up to value $T_{con} = 16.6$ K. Finally, our NbN thin films show very small roughness, which is crucial qualification for the preparation of heterostructures for usage in cryogenic applications.

Acknowledgements

This work was supported by the Slovak Research and Development Agency under the contract no. APVV-16-0315. It is also result of the project implementations: ITMS 26240220027 and 26210120010 supported by the Research & Development Operational Program funded by

the ERDF and grant UK/170/2018 funded by Comenius University.

References

[1] D. Dochev et al, "Growth and characterization of epitaxial ultra-thin NbN films on 3C-SiC/Si substrate for teraherz applications", *Supercond. Sci. Technol.*, vol. 24, pp. 035016, 2011.

[2] E. A. Antonova, D. R. Dzhurgaev, G. P. Motulevich and V. A. Sukhov, "Superconducting energy gap of niobium nitride", *Zh. Exsp. Theor. Fiz.*, vol. 80, pp. 2426–2429, 1981.

[3] E. I. Alessandrini, V. Sadagopan, R. B. Laibowitz, "Relationship between Structure and Sputtering Parameters in NbN Films", *J. Vac. Sci. & Technol.*, vol. 8, pp. 188, 1971.

[4] J. J. Olaya, L. Huerta, S. E. Rodil, R. Escamilla, "Superconducting niobium nitride films deposited by unbalanced magnetron sputtering", *Thin Solid Films*, vol. 516, pp. 8768–8773, 2008.

[5] D. Hazra et al, "Superconducting properties of very high quality NbN thin films grown by high temperature chemical vapor deposition", *Supercond. Sci. Technol.*, vol. 29, pp. 105011, 2016.

[6] S. Linzen et al, "Structural and electrical properties of ultrathin niobium nitride films grown by atomic layer deposition", *Sci. Technol.*, vol. 30, pp. 035010, 2017.

[7] A. Bhat, X. Meng, A. Wong, T. V. Duzer, "Superconducting NbN films grown using pulsed laser deposition for potential application in internally shunted Josephson junctions", *Supercond. Sci. Technol.*, vol. 12, pp. 1030–1032, 1999.

[8] R. E. Treece et al, "Pulsed laser deposition of high-quality NbN thin films", *Appl. Phys. Lett.*, vol. 65, pp. 2860, 1994.

[9] A. B. Kaul, T. D. Sands, T. V. Duzer, "High-Tc superconducting NbN films with low particulate density grown at 25 ° C using pulsed laser deposition", *J. Mater. Res.*, vol. 16, pp. 1223–1226, 2001.

[10] Th. Kehagias, Ph. Komninou, G. Nouet, P. Ruterana, and Th. Karakostas, "Misfit relaxation of the AlN/Al_2O_3 (0001) interface", *Phys. Rev. B*, vol. 64, pp. 195329, 2001.

[11] F. Merciere et al, "Niobium nitride thin films deposited by high temperature chemical vapor deposition", *Surface and Coatings Technology*, vol. 260, pp. 125–132, 2014.

[12] J. Narayan, B. C. Larson, "Domain epitaxy: A unified paradigm for thin film growth", *J. Appl. Phys.*, vol. 93, pp. 278, 2003.

[13] Z. Wang, A. Kawakami, Y. Uzawa, B. Komiyama, "Superconducting properties and crystal structures of singlecrystal niobium nitride thin films deposited at ambient substrate temperature", *J. Appl. Phys.*, vol. 79, pp. 7837–7842, 1996.

[14] J. M. Rowell, S. Y. Xu, X. H. Zeng, A. V. Pogrebnyakov, Q. Li, X. X. Xi, J. M. Redwing, W. Tian, X. Pan, "Critical current density and resistivity of MgB_2 films", *Appl. Phys. Lett.*, vol. 83, pp. 102–104, 2003.

[15] J. R. Clem et al, "Ambegaokar-Baratoff-Ginzburg-Landau crossover effects on the critical current density of granular superconductors", *Phys. Rev. B*, vol. 35, pp. 6637, 1987.

[16] K. Senapati, N. K. Pandey, R. Nagar, R. C. Budhani, "Normal-state transport and vortex dynamics in thin films of two structural polymorphs of superconducting NbN", *Phys. Rev. B*, vol. 74, pp. 104514, 2006.

[17] B. Abeles, "Effect of charging energy on superconductivity in granular metal films", *Phys. Rev. B*, vol. 15, pp. 2828, 1977.

[18] S. Thakoor, J. L. Lamb, A. P. Thakoor, S. K. Khanna, "High T_c superconducting NbN films deposited at room temperature", *J. Appl. Phys.*, vol. 58, pp. 4643, 1985.

[19] T. Shino et al, "Improvement of the critical temperature of superconducting NbTiN and NbN thin films using the AlN buffer layer", *Sci. Technol.*, vol. 23, pp. 045004, 2010.

Received 19 March 2019